様　式　Ｃ－１９、Ｆ－１９－１、Ｚ－１９　（共通）

科学研究費助成事業　　研究成果報告書

平成　２９　年　　６　月　　６　日現在

機関番号：　１２６０１
研究種目：　若手研究(B)
研究期間：　2015～2016
課題番号：　１５Ｋ１７９８４

研究課題名（和文）Synthesis of small diameter single-walled carbon nanotubes and their application in Si heterojunction solar cells

研究課題名（英文）Synthesis of small diameter single-walled carbon nanotubes and their application in Si heterojunction solar cells

研究代表者

項　栄（XIANG, Rong）

東京大学・大学院工学系研究科（工学部）・助教

研究者番号：２０７４００９６

交付決定額（研究期間全体）：（直接経費）　　3,100,000円

研究成果の概要（和文）：単層カーボンナノチューブ（SWNT）は代表的な一次元材料で，多くの面で特異な性質を有している．本プロジェクトでは，SWNT研究の2つの問題に焦点をあてる．第一に，直径およびカイラリティ制御合成を行った．コバルト-銅触媒から直径1nm以下の垂直配向SWNTが得られ，またコバルト-タングステン触媒からは(12,6)カイラリティを豊富に含むSWNTが得られた．第二に，太陽電池において透明導電電極に代わる材料として垂直配向SWNTを導入した．エネルギー変換効率10%を持つ太陽電池が得られ，SWNTの有用性を確かめた，PMMAコーティングを施すことで，この値はさらに12%程度まで向上可能である．

研究成果の概要（英文）：Single-walled carbon nanotubes (SWNTs) are representative 1D nano-material and possess many exceptional properties. Many applications have bee proposed. In this project, we focus on two issues in SWNT research. First, we performed diameter and chirality controlled synthesis of SWNTs. Sub-nm vertically aligned SWNTs are obtained from Co-Cu catalyst, and (12,6) enriched SWNTs are successfully synthesized from sputter Co-W catalyst. Second, we introduced VA-SWNT in a solar cell as the replacement of metal transparent conductive electrode. The SWNTs based are found to be effective in a solar cell with power conversion efficiency of 10%. This value can be further improved to about 12% by putting a PMMA coating layer.

研究分野：　熱工学

キーワード：　カーボンナノ材料　ナノチューブ　合成制御　太陽電池　透過型電子顕微鏡

１．研究開始当初の背景

There have been generally two approaches to use a SWNT film in a solar cell. The first one is to use the metallic component in the film, which simply serves as a transparent conducting film like ITO. The second and more expected approach is to use the energy transition of semi-conducting SWNTs, which is, as just mentioned, tunable by SWNT diameter. In this approach, increasing SWNT band gap to ~1 eV (close to that of Si, 1.1 eV), i.e. reducing SWNT diameter below 1 nm is compulsory to utilize the majority energy in the solar spectrum. Figure 2 shows a Si-SWNT cell we fabricated using SWNTs with an average diameter of 2.5 nm. Since the band-gap is only ~0.4 eV, the contribution of SWNTs on electron-hole generation is very small.[4] If smaller diameter SWNTs are used, the power conversion efficiency is expected to significantly increase.

Partly motivated by the above presented reason, there have been many attempts to control the diameter of SWNTs in a thin film directly from a chemical vapor deposition (CVD) approach. Among these progresses, one of the most successful studies was reported in 2006 by K. Hata Group at AIST, who managed to continuously tune the average diameter of SWNTs from 5 down to 2 nm.[5] However, the band gap of a 2 nm semi-conducting SWNT is only 0.5 eV, which is still far from the expected value (~1 eV) that can be used for efficient solar energy harvesting. By 2012, after a systematic optimization of our Co/Mo catalyst, we succeeded in synthesizing random and vertically aligned SWNTs with diameter tunable from 1.2-2.5 nm.[6] In 2013 we further simplified the catalyst preparation and achieved similar results.[7] At about the same time, Robertson Group at Cambridge Univ. proposed a three layer AlOx/Fe/AlOx catalyst support design that could also produce sub-2 nm SWNT film on flat substrate.[8] Though it is getting closer to the targeting value, producing SWNTs with even smaller diameter (e.g. sub-1.0 nm) using presently available catalysts still remains as a big challenge in the community.

２．研究の目的

The aim of this proposal is as follows.

(1) to synthesize high quality SWNTs with average diameter reduced;
(2) to sub-1.0 nm, to study the growth mechanism behind diameter control
(3) to apply the diameter-reduced SWNTs into a heterojunction solar cell.

３．研究の方法

(1) Prepare of catalyst

The as-received 500-nm-thick Si substrate with 100-μm-thick thermally grown SiO2 (SUMCO) was annealed at 500˚C in air for 30 min to remove possible organic contaminants. The catalysts were loaded on the substrates through dip-coating processes, followed by the calcination at 400ºC in the air. Cobalt nanoparticles were loaded after the supporting catalysts (i.e., copper or molybdenum), although changing the sequences of dip-coating makes no difference in catalytic behaviors, i.e., the quality, yield and diameter distribution of SWNTs.

(2) Growth of SWNTs by ACCVD.

Substrates carrying catalysts were placed in a quartz tube (with the diameter of 26 mm) and annealed under Ar/H2 (3%) environment at the pressure of 40 kPa, from room temperature to target temperature in 30 min. Once the target temperature was reached, the quartz tube was immediately evacuated to the system vacuum of 22 Pa. The substrates were kept at the target temperature, and ethanol feedstock (dehydrated, 99.5%, Wako Chemical, Inc.) was introduced with a flow rate of 50 sccm with the total pressure at 1.3 kPa.

(3) TEM Characterization.

The catalysts samples with TEM grid were kept in the CVD chamber under Ar environment overnight after being reduced by Ar/3% H2 at 650 ˚C. The air exposure from the CVD chamber to the STEM characterization was limited within 1 h. The HAADF-STEM observation was operated at the acceleration voltage of 200 kV. Characterization of particles consisted of HRTEM (200kV, JEM-2000EX, JEOL Co., Ltd.) and STEM-EDS (200kV, JEM-ARM200F Cold-FEG dual SDD, JEOL Co., Ltd.). EDS mapping was carried out by using EDS analyzer (Noran system 7, Thermo Fisher Scientific, Co. Ltd.).

４．研究成果

Figure 1a shows the resonant Raman spectra of SWNTs synthesized by Co/Cu and Co/Mo bimetallic systems under the laser excitation of 488 nm (2.54 eV) and 633 nm (1.96 eV). Here, the Co/Mo bimetallic catalyst system, instead of Co monometallic catalyst system, was used as control group. CoMo800 represents SWNTs synthesized by our conventional growth condition (Co/Mo catalysts with weight ratio of

1:1, under CVD temperature of 800ºC). CoMo800 has very high quality with G/D ratio of 35. Its main radial breathing mode (RBM) peaks distributed in the range of 100 ~ 200 cm-1. According to the RBM (ωRBM) – SWNT diameter (dt) relationship ωRBM = 217.8/dt + 15.7, the average diameter of CoMo800 was estimated as 1.8 nm. When the CVD temperature was decreased to 650ºC, the quality of the as-synthesized SWNTs (CoMo650) was significantly reduced, with G/D ratio of only 8. The RBM peaks of CoMo650 distributed widely in the range of 100 ~ 300 cm^{-1}. This is in agreement with previous reports that reducing CVD temperature could decrease the diameter of SWNTs in the price of lower quality. Surprisingly, by using Co/Cu bimetallic catalyst system (weight ratio = 1:1) under the same CVD temperature of 650 ºC, the as-synthesized SWNTs (CoCu650) possessed both subnanometer diameter and high quality. The RBM peaks of CoCu650 narrowly distributed in the range of 250 ~ 300 cm-1, and its average diameter was estimated as 0.75 nm. G band also exhibited the small diameter of both the semiconducting and metallic nanotubes in CoCu650. The remarkable separation of G+ and G- modes as well as the <1540 cm-1 G- mode confirmed the subnanometer diameter of the semiconducting nanotubes in CoCu650; while the Breit–Wigner–Fano (BWF) lineshape demonstrated the subnanometer diameter of the metallic nanotubes in CoCu650.

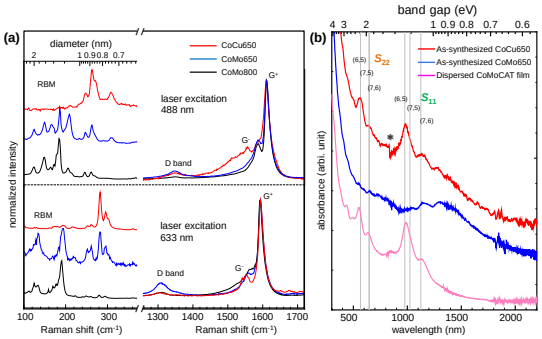

Figure 1. (a) Raman spectra of as-synthesized CoCu650, CoMo650 and CoMo800, measured by laser excitation of 488 nm and 633 nm. (b) UV-vis-NIR absorption spectra of CoCu650, CoMo650 and dispersed CoMoCAT film. The chirality species of (6,5), (7,5) and (7,6) are indicated. The asterisk marks the step caused by the lamp change from near-infrared to visible spectrum.

To examine the compositions of the nanoparticles in the Co/Cu bimetallic catalyst system (CVD temperature of 650 ºC), we further conducted elements mapping of Co and Cu by using STEM EDS. The results are shown in Figure 2a and 2b. The element mapping demonstrated that the distribution of Co (magenta) was similar to GCo/Cu-S, while the distribution of Cu (cyan) was similar to GCo/Cu-L. Interestingly, when overlapping the element distributions of Co and Cu, it could be observed that each GCo/Cu-L nanoparticle was actually a binary particle system where a Co nanoparticle was anchored by a Cu nanoparticle, as shown in Figure 2c. Note that Co was not fully surrounded by Cu, but partially exposed on the surface of the GCo/Cu-L nanoparticle. Moreover, neither alloys nor intermetallic compounds could be solidly recognized, owing to the very low mutual solubility (<1%) of Co and Cu at 650 ºC. The formation of the binary particle system was mainly attributed to the well-known strong adhesion force between Co and Cu. The strong Co-Cu adhesion force has been widely utilized in semiconductor industries, in which the expansion and diffusion of Cu particles could be effectively limited by adding Co particles. In this research, owing to the strong Co-Cu adhesion force, Co nanoparticles were quickly captured anchored by nearby Cu nanoparticles before being coalesced into larger Co nanoparticles. The small Co nanoparticles protected by Cu resulted in the subnanometer diameter of the SWNTs.

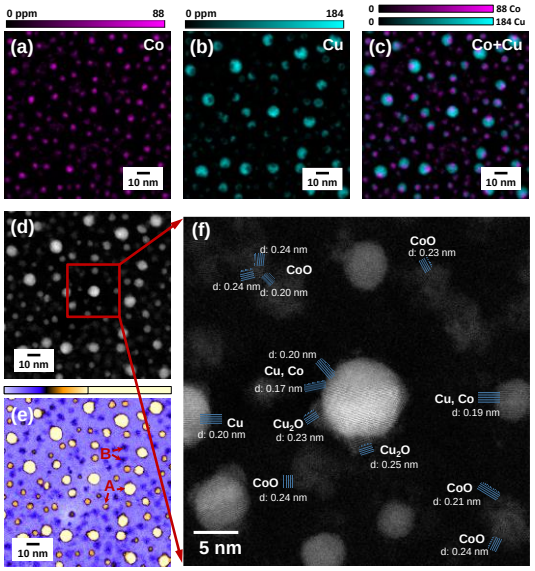

Figure 2. EDS elemental mapping of (a) Co and (b) Cu on the surface of Co/Cu catalysts. (c) Combinational image of (a) and (b) showing Co nanoparticles are anchored by Cu. (d) HAADF-STEM imaging of the Co/Cu catalyst with (e) highlight intensity distribution using color bar. The imaging was taken in the same area shown in (a-c). (f) High-resolution HAADF-STEM micrograph of (d).

Moreover, the chemical status of the nanoparticles in the Co/Cu bimetallic catalyst system was examined by HAADF-STEM. The imaging intensity of HAADF-STEM is strongly dependent on the atomic number (Z) of the constituent atoms.33,34 The Z-contrast imaging micrographs shown in Figure 2d and 2e were taken in the same area shown in Figure 2c. As the

atomic numbers of Co (Z=27) and Cu (Z=29) are almost the same, a brighter contrast is caused by denser atoms or thicker specimen, i.e., a larger particle. If we focus on the same particle size, the difference of the HAADF contrast should only depend on the density of atoms. Because the metal densities of Co/Cu is approximately two times of that of oxide, the metallic nanoparticles (arrow A in Figure 2e) are much brighter than oxide ones (arrow B in Figure 2e). The Co nanoparticles anchored by Cu nanoparticles were consistent with the bright HAADF contrast derived from metallic nanoparticles, while the nanoparticles consisting of only Co were oxidized with the dark HAADF contrast. As shown by the high-resolution HAADF-STEM image in Figure 2f, the GCo/Cu-S nanoparticles exhibited lattice distances ranging from 0.21 ~ 0.24 nm, which corresponded to the CoO (200) lattice constant. Moreover, a typical GCo/Cu-L nanoparticle in the center of Figure 2f was identical to the single-like crystal with fcc structure, which indicated that there was no twin or any planar defects between Co and Cu crystalline in this nanoparticle. The perfect grain boundary between Co and Cu illustrated by HAADF-STEM may be the main reason for their strong adherence which results in the anchoring effect of Cu.

After obtaining sub-nm VA-SWNTs from Co/Cu catalyst, we further performed chirality specific growth using Co/W catalyst.

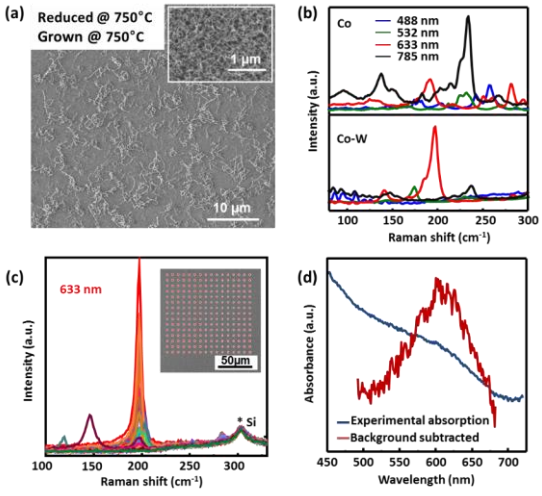

(e)

Excitation laser wavelength (nm)	488	532	633	785	total
Number of RBM peaks	21	161	952	23	1157
Number of (12,6) peaks (~197 cm⁻¹)	0	0	607	0	607
Proportion of (12,6) peak among all RBM= 607/1157=53%					
Calibrated enrichment of (12,6) among all SWNTs=75%					

Figure 3. Characterization of SWNTs grown from sputtered CoW. (a) A typical SEM image of SWNTs grown from CoW inset with the SWNTs arrays obtained from pure Co. (b) Averaged Raman spectra in RBM region of SWNTs grown from pure Co and CoW with four different excitation wavelengths. (c) Raman spectra of SWNTs with multi data excited at 633 nm. (d) An optical absorption spectrum of SWNT samples after dispersion. (e) Statistical analysis on SWNTs of (12, 6) with RBM occurrence frequencies excited by four lasers: 488, 532, 633 and 785 nm.

Figure 3a shows a representative SEM image of the as-grown SWNTs formed at a growth temperature of 750ºC. A sample grown from pure Co at the same condition is shown as the inset for comparison. Without the existence of W, SWNTs form into a thick mat with a high nucleation density, while in case of Co-W, SWNT density decreases significantly. The length of SWNTs obtained from Co-W after a 5 min growth is usually several micrometers according to higher resolution SEM and TEM observations, which shows no much difference from those obtained from pure Co. Raman spectroscopy is used to confirm the existence and the structure of SWNTs. The G-band of both samples (grown from Co and Co-W catalyst) shows typical features of SWNTs, with a clear split into G^+ and G^-. D band of both samples are not strong, and typical G/D ratios are about 15 to 20 (Figure S1). However, clear differences are observed between two samples in Radial Breathing Mode (RBM) regions (Figure 1b). In the case of pure Co, RBM peaks from four laser excitations demonstrate a wide distribution, while for Co-W, though SWNTs with other chiralities also exist, the peak locating at 197 cm^{-1} excited by 633 nm laser becomes dominant. The index of the dominant SWNTs is assigned to be (12, 6) according to the diameter and the excited transition energy in the Kataura plot.

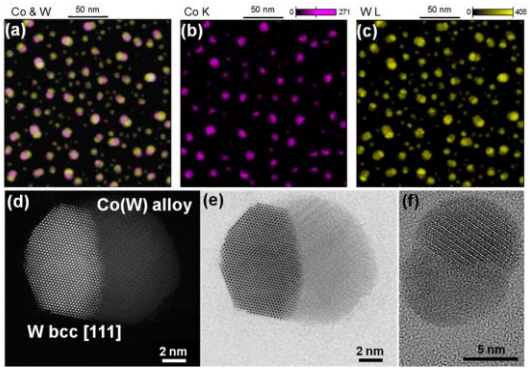

Figure 4. Elemental distribution mapping and high resolution STEM images of the as-reduced Co-W catalyst at 850ºC. (a) Overlapped Co and W distribution, (b) Co distribution, (c) W distribution, (d) High resolution HAADF image of the W-Co6W6C junction, (e) High resolution STEM bright field image of the W-Co6W6C junction, (f) Cs-TEM image of the W-Co6W6C junction.

Finally we applied SWNTs in a solar cell. SWNT-applied metal-free PSCs produced a PCE

of 10.0% even in the absence of HTMs. This was due to the fact that the perovskite layer (CH3NH3PbI3) can partially function as a transporting material. SWNT films have also been reported to have some hole-transporting effect. A simple over-coating of SWNT film with a solution of PMMA improved the PCE by around 2%. This improvement was due to increases in all three photovoltaic parameters, VOC, JSC, and FF. From the photovoltaic data and current-voltage (J−V) curves, we observed that the difference between forward and reverse J−V curves was much reduced (Figure 5a). This indicates that the application of PMMA reduced hysteresis. Cross-sectional scanning electron microscopy (SEM) pictures in Figure 6c-f show the interface between SWNT film and the perovskite layer. Before chlorobenzene was applied, some parts of the SWNT film did not make contact with the perovskite layer (Figure 5d). After the chlorobenzene application, magnified SEM picture showed that the SWNT film makes full contact with the perovskite layer. Form Figure 5f, we can see that the addition of PMMA densifying the SWNTs. Polymeric gel-like PMMA seem to have percolated into the SWNTs, filling the air gaps inside the network and reduced the thickness of the SWNT film. From the J−V curves in Figure 5a, we can see that the application of PMMA induced less noise and reduced hysteresis. The reduction in hysteresis can also be explained by decreased trapped charge in the SWNT film. According to the study conducted by Choi and colleagues, hysteresis is caused by trapped charge at the interface of perovskite layer and can be reduced by effective charge extraction. It is our belief that SWNTs densified by PMMA can extract trapped charge more effectively.

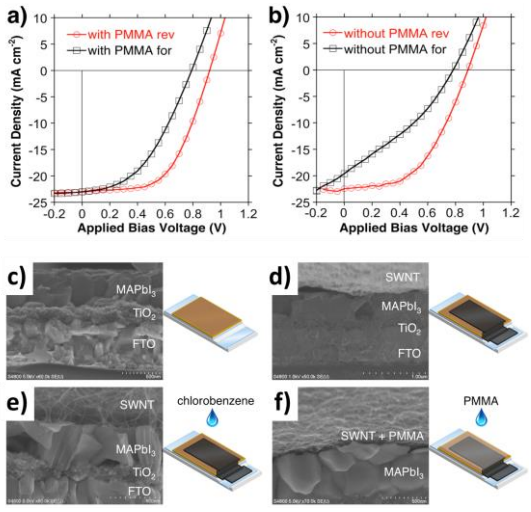

Figure 5. J–V curves of (a) a SWNT film-laminated PSC with PMMA and (b) the same SWNT film-laminated PSC without PMMA under AM 1.5G one sun illumination (100 mW/cm2). (The aperture mask area was 0.1 cm2 with a scan rate of 200 ms from 1.2 V to -0.2 V. Reverse bias was measured first followed by forward bias); Cross-sectional SEM pictures of (c) a PSC without HTM and metal electrode, (d) a SWNT film-laminated PSC before chlorobezene addition, (e) a SWNT film-laminated PSC after chlorobezene addition, and (f) a SWNT film-laminated PSC after PMMA addition.

５．主な発表論文等
（研究代表者、研究分担者及び連携研究者には下線）

〔雑誌論文〕（計　11　件）

[1] S. Yoshida, Y. Feng, T. Inoue, **R. Xiang**, S. Chiashi, E. I.Kauppinen, S. Maruyama*, Morphology Dependence of the Thermal Transport Properties of Single-Walled Carbon Nanotube Thin Films, Nanotechnology, (2017), 28-18, 185701-1-185701-7. 査読有

[2] B. Hou, C. Wu, T. Inoue, S. Chiashi, **R. Xiang***, S. Maruyama*, Extended Alcohol Catalytic Chemical Vapor Deposition for Efficient Growth of Single-walled Carbon Nanotubes Thinner than (6,5), Carbon, (2017), 119, 502-510. 査読有

[3] H. An, A. Kumamoto, H. Takezaki, S. Ohyama, Y. Qian, T. Inoue, Y. Ikuhara, S. Chiashi, **R. Xiang***, S. Maruyama*, Chirality specific and spatially uniform synthesis of single-walled carbon nanotubes from sputtered Co-W bimetallic catalyst, Nanoscale, (2016), 8, 14523-14529. 査読有

[4] X. Chen, **R. Xiang***, P. Zhao, H. An, T. Inoue, S. Chiashi, S. Maruyama*, Chemical Vapor Deposition Growth of Large Single-crystal Bernal-stacked Bilayer Graphene from Ethanol, Carbon, (2016), 107, 852-856. 査読有

[5] I. Jeon, Y. Qian, S. Nakao, D. Ogawa, **R. Xiang**, T. Inoue, S. Chiashi, T. Hasegawa, S. Maruyama*, Y. Matsuo*, Room Temperature-processed Inverted Organic Solar Cells using High Working-Pressure-Sputtered ZnO film, J. Mater. Chem. A, (2016), 4, 18763-18768. 査読有

[6] Y. Song, J. Zhuang, M. Song, S. Yin, Y. Cheng, X. Zhang, M. Wang, **R. Xiang**, Y. Xia, S. Maruyama, P. Zhao*, F. Ding, H. Wang, Epitaxial nucleation of CVD bilayer graphene on copper, Nanoscale, (2016), 8, 20001-20007. 査読有

[7] A. Westover, J. Choi, K. Cui, T. Ishikawa, T. Inoue, **R. Xiang**, S. Chiashi, T. Kato, S. Maruyama*, C. Pint*, Load Dependent

Frictional Response of Vertically Aligned Single-Walled Carbon Nanotube Films, Scripta Mater., (2016), 125, 63-67. 査読有

[8] K. Cui, A. Kumamoto, **R. Xiang**, H. An, B. Wang, T. Inoue, S. Chiashi,Y. Ikuhara, S. Maruyama*, Synthesis of subnanometer-diameter vertically aligned single-walled carbon nanotubes with copper-anchored cobalt catalysts, Nanoscale, (2016), 8-3, 1608-1617. 査読有

[9] R. Kitaura, Y. Miyata, **R. Xiang**, J. Hone, J. Kong, R. S Ruoff, S. Maruyama*, Chemical Vapor Deposition Growth of Graphene and Related Materilas, *J. Phys. Soc. Jpn.*, (2015), 84, 121013-1-13. 査読有

[10] Y. Won, Y. Gao, R. Guzman de Villoria, B. L. Wardle, **R. Xiang**, S. Maruyama, T. W. Kenny, K. E. Goodson*, Nonhomogeneous Morphology and the Elastic Modulus of Aligned Carbon Nanotube Films, *J. Micromech. Microeng.*, (2015), 25, 115023-1-7. 査読有

[11] X. Chen, P. Zhao, **R. Xiang**, S. Kim, J. Cha, S. Chiashi, S. Maruyama*, Chemical Vapor Deposition Growth of 5 mm Hexagonal Single-Crystal Graphene from Ethanol, Carbon, (2015), 94, 810-815. 査読有

〔学会発表〕（計　6　件）

[1] **Rong Xiang**, Controlled synthesis of single-walled carbon nanotubes using alcohol catalytic chemical vapor deposition - Visualization of catalyst directly on SiO2 by In-plane TEM, 2017.3.19-3.22, Kyushu University, Fukuoka, Japan.

[2] **Rong Xiang**, Akihito Kumamoto, Hua An, Taiki Inoue, Shohei Chiashi, Yuichi Ikuhara, Shigeo Maruyama, Bimetallic Catalyst for Chirality and Diameter Controlled Growth of Single-walled Carbon Nanotubes, 2016.11.15-11.18, Tokyo Institute of Technology, Meguro-ku, Tokyo, Japan.

[3] **Rong Xiang**, Akihito Kumamoto, Hua An, Taiki Inoue, Shohei Chiashi, Yuichi Ikuhara, Shigeo Maruyama, In-Plane TEM Imaging of Bimetallic Catalyst for SWNT Growth, The 51st Fullerenes-Nanotubes-Graphene General Symposium, September 07 (Wed.) - 09 (Fri.), 2016, Hokkaido citizens actives center, Sapporo, Hokkaido.

[4] **Rong Xiang**, Kehang Cui, Akihito Kumamoto, Hua An, Taiki Inoue, Shohei Chiashi, Yuichi Ikuhara, Shigeo Maruyama, Modulating diameter of single-walled carbon nanotubes in alcohol catalytic chemical vapor deposition, 2015.12.15-12.20, Honolulu, Hawaii, USA.

[5] **Rong Xiang**, Akihito Kumamoto, Kehang Cui, Hua An, Yang Qian, Taiki Inoue, Shohei Chiashi, Yuichi Ikuhara, Shigeo Maruyama, In-plane TEM investigation on mono- and bi- metallic catalyst for growth of single walled carbon nanotubes, 2015.9.7-9.9, Kitakyushu International Conference Center, Kita-Kyushu, Fukuoka Prefecture, Japan.

[6] **Rong Xiang**, Kehang Cui, Akihito Kumamoto, Hua An, Taiki Inoue, Shohei Chiashi, Yuichi Ikuhara, Shigeo Maruyama, Modulating diameter of single-walled carbon nanotubes in alcohol catalytic chemical vapor deposition, 2015.6.29-7.3, Nagoya University, Nagoya, Aichi Prefecture, Japan.

〔図書〕（計　　件）
〔産業財産権〕

○出願状況（計　　件）

名称：
発明者：
権利者：
種類：
番号：
出願年月日：
国内外の別：

○取得状況（計　　件）

名称：
発明者：
権利者：
種類：
番号：
取得年月日：
国内外の別：

〔その他〕
http://www.photon.t.u-tokyo.ac.jp/~xiangrong/

６．研究組織
(1)研究代表者
項　栄　　（ XIANG Rong ）
東京大学・大学院工学研究科・助教
研究者番号：２０７４００９６

(2)研究分担者
（　　）
研究者番号：

(3)連携研究者
丸山　茂夫　（ MARUYAMA Shigeo ）
東京大学・大学院工学研究科・教授
研究者番号：９０２０９７００

(4)研究協力者
（　　）